Flexible modelling of the dissolution performance of directly compressed tablets

Natalie Maclean [a,b], John A. Armstrong [a,b], Mark A. Carroll [a,b], Mohammad Salehian [a,b], James Mann [c], Gavin Reynolds [c], Blair Johnston [a,b], Daniel Markl [a,b,*]

[a] Centre for Continuous Manufacturing and Advanced Crystallisation (CMAC), University of Strathclyde, Glasgow, UK
[b] Strathclyde Institute of Pharmacy & Biomedical Sciences, University of Strathclyde, Glasgow, UK
[c] Oral Product Development, Pharmaceutical Technology & Development, Operations, AstraZeneca, Macclesfield, UK

ARTICLE INFO

ABSTRACT

In this study, a compartmental disintegration and dissolution model is proposed for the prediction and evaluation of the dissolution performance of directly compressed tablets. This dissolution model uses three compartments (Bound, Disintegrated, and Dissolved) to describe the state of each particle of active pharmaceutical ingredient. The disintegration of the tablet is captured by three fitting parameters. Two disintegration parameters, β_0 and $\beta_{t,0}$, describe the initial disintegration rate and the change in disintegration rate, respectively. A third parameter, α, describes the effect of the volume of dissolved drug on the disintegration process. As the tablet disintegrates, particles become available for dissolution. The dissolution rate is determined by the Nernst-Brunner equation, whilst taking into account the hydrodynamic effects within the vessel of a USP II (paddle) apparatus. This model uses the raw material properties of the active pharmaceutical ingredient (solubility, particle size distribution, true density), lending it towards early development activities during which time the amount of drug substance available may be limited. Additionally, the strong correlations between the fitting parameters and the tablet porosity indicate the potential to isolate the manufacturing effects and thus implement the model as part of a real-time release testing strategy for a continuous direct compression line.

1. Introduction

In recent years, the pharmaceutical industry has identified the need to shift towards agile and flexible development and manufacturing practices in order to achieve faster delivery of crucial new treatments, whilst lowering development and manufacturing costs (Kapoor et al., 2021). To achieve this aim, an integrated approach to drug product development is needed, where process and product understanding is combined with advanced measurement and characterisation techniques, and flexible, dynamic models for predicting both process and product attributes (Markl et al., 2020).

A crucial aspect of the development and manufacture of pharmaceuticals is dissolution testing, as the dissolution performance of a product is typically considered a critical quality attribute (CQA) for solid oral dosage forms (ICH, 2009). During the development of a new product, dissolution studies are used to screen and optimise the formulation and manufacturing processes, as well as to select suitable packaging to ensure the dissolution performance is maintained throughout the shelf-life of the product. Dissolution data is essential to regulatory filings, including the registration of a new drug product or to demonstrate

bioequivalence between a generic product and the innovator product. After approval, the dissolution performance of commercial batches must be continuously monitored to ensure that newly manufactured tablets meet the specification required for release (FDA, 1997).

Hence, comprehending the factors impacting dissolution testing is vital. This understanding serves a dual purpose: initially, in developing a robust formulation and manufacturing process, and subsequently, in establishing a reliable dissolution method. Besides the dissolution of the active pharmaceutical ingredient (API), the drug release from a tablet is heavily influenced by its disintegration process. Both the disintegration and drug dissolution processes are initiated by the tablet coming into contact with liquid, which will penetrate the tablet through pores in the microstructure. Most immediate-release tablets contain a low concentration of disintegrant to promote rapid disintegration of the tablet. Disintegrants are typically hygroscopic polymers which absorb large quantities of liquid and expand. Swelling disintegrants (for example, croscarmellose sodium (CCS) or sodium starch glycolate (SSG)) expand omnidirectionally. Shape recovery disintegrants (for example,

Nomenclature

α	The feedback effect of the volume of drug dissolved on the disintegration process (model fitting parameter)
β	Disintegration rate (model fitting parameter)
β_0	Initial disintegration rate (model fitting parameter)
$\beta_{t,0}$	Decay rate for the disintegration rate (model fitting parameter)
ϵ	Power input of USP II apparatus
$\lambda_j(t)$	Radius of particle j at time t
μ_T	Dynamic viscosity at temperature, T
v	Kinematic viscosity of media
ω	USP II paddle speed
ρ_s	True density of the API
$\rho_{f,T}$	Density of the liquid at temperature, T
A_i	Surface area available for dissolution
B_i	Number of particles in the 'Bound' compartment of size bin, i
$C_{S,u}$	Solubility of the API in the dissolution media under the method temperature
C_u	Concentration of API in the dissolution media
$d_{CE,i}$	The circle equivalent diameter of particles in size bin, i
D_p	Diameter of USP II paddle
D_u	Diffusion coefficient
g	Gravitational acceleration at the surface of the Earth
$h_{t,i}$	Thickness of the unstirred media layer
k	Boltzmann constant
L_i	Number of particles in the 'Disintegrated' compartment of size bin, i
M_w	Molecular weight of the API
$m_{t,m}$	Mass of a particle, m, at time, t
N	Avogadro's number
n_i	Total number of API particles in size bin, i
P_0	USP II power number
r_h	Hydrated radius of an API particle
R_i	Number of particles in the 'Dissolved' compartment of size bin, i
r_i	Radius of a particle in size bin, i
$r_{i,0}$	Initial radius of a particle in size bin, i
$r_{t,i,j}$	Radius of particle, j, in size bin, i, at time, t
Re_p	Reynolds number of particle, p, in the vessel
Sc	Schmidt number
Sh	Sherwood number
T	Temperature
t	Timepoint in the dissolution process
V_d	Volume of dissolved API particles
V_L	Volume of dissolution media in the vessel
v_m	Relative velocities due to micro-eddies
V_t	Total volume of API particles
v_t	Particle slip velocity
$v_{r,t}$	Velocity of the particle in the fluid
$x_{v,d}$	Fraction of the volume of dissolved API particles

crospovidone (XPVP)) expand uni-directionally against the direction of compression. Both of these mechanisms result in the generation of a swelling force which acts against the surrounding tablet matrix to break the tablet apart into smaller fragments. As the tablet disintegrates, the surface area available for dissolution increases. During dissolution, solvation occurs on the surface of exposed particles, and molecular bonds within the API break as the molecules diffuse into the bulk solution. The disintegration of tablets has been discussed in several recent reviews (Quodbach and Kleinebudde, 2015; Desai et al., 2016; Markl and Zeitler, 2017; Berardi et al., 2021).

The dissolution performance of a pharmaceutical product is influenced by the raw material properties of the API and excipient powders, the bulk powder properties, the manufacturing and coating process, the properties of the final drug product, the dissolution medium and the dissolution testing conditions. The relative effect of these factors on the dissolution rate will depend on the mechanisms driving the disintegration and dissolution. For example, Wilson et al. (2012) coupled particle size analysis with a standard USP II apparatus to demonstrate the difference in mechanism for two formulations — one which was limited by the tablet disintegration, and the other was limited by the intrinsic dissolution rate of the API. Similarly, assessment of 16 different placebo formulations showed that the effect of porosity and disintegrant concentration on the disintegration time depended on the performance-controlling mechanism (Maclean et al., 2021). Depending on the performance-controlling mechanism (e.g. wettability controlled, dissolution controlled, or swelling controlled), the disintegration and dissolution performance may be sensitive to the tablet porosity, the disintegrant concentration, or the excipient selection and composition. The role of porosity and tablet microstructure in the disintegration and dissolution performance of tablets was recently reviewed by Jange et al. (2023).

In recent years, several different approaches have been explored to enable predictive dissolution modelling for product development and real-time release testing. Advances in the field of process analytical technology (PAT) has enabled rapid, non-destructive at-line measurements during the manufacturing process. In particular, near infrared (NIR), Raman, and terahertz time-domain spectroscopy (THz-TDS) have been used as non-destructive, at-line – and some on-line and in-line – measurements to characterise pharmaceutical products. Several groups have used multivariate analysis such as partial least squares (PLS) regression to develop dissolution models based on NIR and Raman spectroscopic data (Dumarey et al., 2015; Freitas et al., 2005; Hernandez et al., 2016). Machine learning has also been used to develop dissolution models, for example, Matsunami et al. (2023) developed a surrogate model for dissolution using random forest regression for a wet granulated product. Artificial neural networks have been developed to predict the dissolution performance of extended-release HPMC-based tablets (Galata et al., 2019, 2021, 2022; Péterfi et al., 2023; Nagy et al., 2023). Similarly, Galata et al. (2023) used convolutional neural networks to predict the dissolution profile of extended-release tablets using Raman imaging of the tablet surface. Recently, optical coherence tomography (OCT) images were used to develop a machine learning model for dissolution prediction by Fink et al. (2023). Alternative approaches to dissolution modelling include a reduced-order generalised Weibull model proposed by Ferdoush and Gonzalez (2023), and population balance models (Wilson et al., 2012; Djukaj et al., 2022). A recent review by Zaborenko et al. (2019) discussed first-principle and empirical approaches to dissolution modelling for both development and release testing.

The drawback of approaches which use multivariate analysis or machine learning is that they are typically inflexible and restrictive in their application. To develop these models, large amounts of data are required to develop or train the models. This may be feasible during the later stages of development or as part of a real-time release testing strategy, where the formulation and manufacturing processes are fixed. During the early stages of development, where there may still

Table 1
The formulations of ibuprofen and indomethacin tablets manufactured by Bawuah et al. (2021). Further details on the formulations and manufacturing can be found in the appropriate reference. Abbreviations: MCC — microcrystalline cellulose; LAC — lactose; CCS — croscarmellose sodium; MgSt — magnesium stearate.

Label	API		Fillers				Disintegrant		Lubricant	
	Material	% wt.	Material	% wt.	Material	% wt.	Material	% wt.	Material	% wt.
F1	Ibuprofen	1.0	MCC	43.2	LAC	51.8	CCS	3.0	MgSt	1.0
F2	Ibuprofen	10.0	MCC	39.1	LAC	46.9	CCS	3.0	MgSt	1.0
F3	Indomethacin	1.0	MCC	43.2	LAC	51.8	CCS	3.0	MgSt	1.0
F4	Indomethacin	10.0	MCC	39.1	LAC	46.9	CCS	3.0	MgSt	1.0

be changes to the product, it is unlikely that sufficient data would be available for these approaches. These types of models are often specific to one API or product, and would not be transferrable when developing a new drug product.

In this study, a compartmental disintegration and dissolution model is proposed to define and predict the dissolution profiles of directly-compressed tablets. In this model, the difference between the dissolution of the API powder and the dissolution of API from a formulated tablet is attributed to particles being bound in the tablet (i.e. not yet disintegrated), and therefore not yet available to dissolve. The dissolution model is demonstrated for batches of ibuprofen and indomethacin tablets, across a range of porosity levels with two drug loadings (1 and 10% wt.).

2. Materials and methods

2.1. Materials

This study uses data previously published by Bawuah et al. (2021) to demonstrate the application of the dissolution model. Further details of the materials, and the manufacture and characterisation of tablets can be found therein. Two different APIs were investigated: ibuprofen (CAS 15687-27-1, 99.9%) from BLD Pharmatech Ltd (Hong Kong) and indomethacin (CAS 53-86-1, 98.5–100.5%) from Merck (Gillingham, UK). The ibuprofen and indomethacin tablets contained microcrystalline cellulose (MCC, Avicel PH-102®, FMC Europe NV), lactose anhydrous (Supertab® 21AN, DFE Pharma), croscarmellose sodium (CCS, DuPont Nutrition), and magnesium stearate (Fisher Scientific).

2.2. Methods

2.2.1. Raw material characterisation

The particle size distribution, solubility, and true density of the API are required as inputs for the dissolution model. These properties were measured experimentally, as described in Section 1 of the Supporting Information.

2.2.2. Tablet manufacture

Full details of the manufacture of all tablets are provided by Bawuah et al. (2021). A summary of the formulations of each batch is shown in Table 1. Briefly, all tablets were manufactured by direct compression. Round, biconvex tablets of 10 mm diameter were manufactured with a target weight of around 400 mg. The compression force was varied between batches to achieve varying levels of porosity.

2.2.3. Tablet characterisation

The experimental data for the tensile strength, disintegration time, and dissolution performance of tablets was previously published by Bawuah et al. (2021). The porosity of the tablets was calculated as described in the Supporting Information. The dissolution test method used by Bawuah et al. (2021) is summarised in Table 2, whilst a summary of the tablet porosity and disintegration time is given in Table 3.

2.2.4. Data preparation

The dissolution model uses the particle size distribution (PSD) of the API as an input. The PSD of each API was measured using Morphologi G3 (Malvern Instruments Ltd, Worcestershire, UK), as described in the Supporting Information. The PSD was then divided into a number of bins, and the number of particles within the bin for each representative size, i, is determined (Figure S1 in the Supporting Information). Due to the wide particle size distributions of indomethacin and ibuprofen, the bin sizes were determined by using log-spacing to divide particles between the minimum and maximum circle equivalent (CE) diameter. For each bin, the particles within that bin are considered to have a starting radius ($r_{i,0}$) based on the CE diameter. In this study, the full particle size distributions of ibuprofen and indomethacin were each divided into 10 bins.

2.3. The dissolution model

A compartmental disintegration and dissolution model is proposed which uses population balance principles to monitor the state of individual API particles during the disintegration and dissolution process (Fig. 1). Several basic assumptions underlie the dissolution model:

- The particles are treated as spheres.
- The API particles are homogeneously distributed throughout the tablet.
- Disintegration of the tablet results in the liberation of primary particles of API.
- Only particles released by disintegration are available for dissolution.

2.3.1. The compartmental model

This model is adapted from the compartmental SIR model, which is used in the field of epidemiology to model disease transmission during pandemics by considering individuals as being either susceptible, infected or removed (Weiss, 2013). The presented model uses a population-balance approach, using three "compartments" to describe the different stages of the dissolution process. The Bound compartment, B, describes particles which are still bound in the intact tablet, i.e. particles which have not yet disintegrated and so are not considered available for dissolution. For each particle size bin, all particles begin in the Bound compartment at $t = 0$. When the tablet begins to disintegrate, particles will be liberated from the tablet and move from the Bound compartment to the Disintegrated (L) compartment. In this compartment, particles have been liberated from the intact tablet and are now considered available for dissolution and will remain in this compartment until fully dissolved. Once the particle has fully dissolved, it moves to the final compartment, Dissolved (D).

For each particle size bin, i, all particles begin in the B_i compartment with radius, $r_{i,0}$. This radius is determined based on the CE diameter after binning the full particle size distribution of the API (as described in Section 2.2.4 and in the Supporting Information).

The movement of particles between compartments is described by the following system of coupled ordinary differential equations:

$$\frac{dB_i}{dt} = -\beta(t)B_i(t) - \alpha x_{V,d}(t)B_i(t), \qquad (1)$$

Table 2

A summary of the dissolution methods used by Bawuah et al. (2021) to collect experimental dissolution data for ibuprofen and indomethacin tablets. All dissolution testing was performed using USP II (paddle) apparatus with 900 mL of dissolution media in each vessel. During sampling, media was recycled after analysis to maintain constant volume in the vessel.

Batch	Dissolution media	Temperature	Paddle speed	Sampling times
Ibuprofen	pH 7.2 phosphate buffer[a]	37 °C	50 rpm	Every 80 s
Indomethacin	pH 6.2 phosphate buffer[a]			until at least 98% dissolved

[a] Phosphate buffer prepared according to the British Pharmacopoeia.

Table 3

The porosity and disintegration time of tablets containing ibuprofen and indomethacin, reported by Bawuah et al. (2021).

Batch		Porosity (%)	Disintegration time (s)
Ibuprofen 1%	B1	7.43	254
	B2	10.77	128
	B3	17.37	17
	B4	22.25	9
	B5	25.46	7
Ibuprofen 10%	B1	7.38	398
	B2	12.17	147
	B3	16.31	28
	B4	20.86	12
	B5	23.13	12
Indomethacin 1%	B1	6.87	499
	B2	10.99	264
	B3	16.05	95
	B4	21.38	22
	B5	25.73	14
Indomethacin 10%	B1	7.36	419
	B2	11.61	203
	B3	16.31	50
	B4	21.59	13
	B5	25.09	11
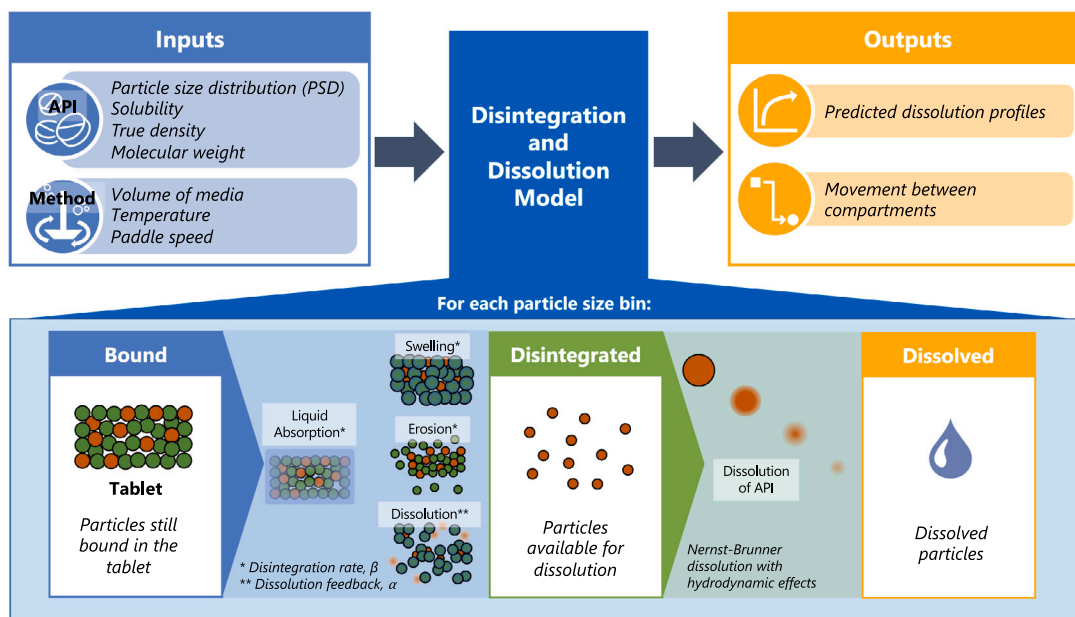
Fig. 1. A schematic summary of the disintegration and dissolution model. The model uses the raw material properties of the API and the dissolution test conditions as inputs. The disintegration and dissolution process is modelled using three compartments, and the progress of particles through the compartments is controlled by population balance modelling. The model returns predictions of the dissolution profile, as well as information on the movement of particles between the three compartments for each particle size bin.

$$\frac{dL_i}{dt} = \beta(t)B_i(t) + \alpha x_{V,d}(t)B_i(t) - \frac{dD_i(t)}{dt}, \qquad (2)$$

where $B_i(t)$, $L_i(t)$ and $D_i(t)$ describe the number of particles in the Bound, Disintegrated and Dissolved compartments at time t, respectively, β is a parameter which describes the disintegration rate, α is a parameter which describes the feedback effect of the drug which has already dissolved on the disintegration rate, and $x_{V,d}$ is the volume fraction of drug which has already dissolved, given by:

$$x_{V,d} = \frac{V_d(t)}{V_t}, \qquad (3)$$

where V_t is the total volume of all API particles within the tablet and $V_d(t)$ is the sum of the volume of dissolved API particles across all size

bins, i, given by the following equations:

$$V_t = \sum_i n_i \frac{4}{3} \pi r_i{}^3, \tag{4}$$

$$V_d(t) = \sum_i D_i(t) \frac{4}{3} \pi r_i{}^3, \tag{5}$$

where n_i is the total number of API particles in the i size class, and $D_i(t)$ is the number of particles in the dissolved compartment of the i size class at time, t.

The system of equations is solved for $B_i(t)$, $L_i(t)$ and $D_i(t)$ using the Euler method. The system is treated as an initial value problem (IVP) with initial conditions $B_i(t = 0) = n_i$ and $L_i(t = 0) = D_i(t = 0) = 0$.

2.3.2. The disintegration process

The disintegration rate, β, is a key aspect of the model. This term describes the rate of liquid uptake and swelling in the tablet. In this paper, we consider the disintegration rate as an exponential process:

$$\frac{d\beta}{dt} = -\beta_{t,0} \beta(t), \tag{6}$$

where $\beta_{t,0}$ is the decay rate. The analytical solution is an exponential decay:

$$\beta = \beta_0 \exp(-\beta_{t,0} t), \tag{7}$$

where β_0 is the initial disintegration rate at $t = 0$. Both β_0 and $\beta_{t,0}$ can be determined by optimising the model against experimental data.

2.3.3. The drug dissolution process

The dissolution model applies the Nernst-Brunner equation to determine the mass of drug dissolved over time, $m_{s,i}$ (Brunner, 1904):

$$\frac{dm_{s,i}}{dt} = A_i(t) \left(\frac{D_u}{h_{t,i}} \right) (C_{S,u} - C_u(t)) \tag{8}$$

where $A_i(t)$ is the surface area available for dissolution, D_u is the diffusion coefficient, $h_{t,i}$ is the thickness of the unstirred media layer, $C_{S,u}$ is the solubility of the API in the dissolution medium, $C_u(t)$ is the concentration of API in the solution at time, t.

In this disintegration and dissolution model, each particle size bin is treated independently. For a given size class, i, the sum of particle sin B_i, L_i, and D_i must always equal the total number of particles for that size class at $t = 0$, i.e. n_i. At a given time step, if the mass dissolved is equal to, or greater than, the mass of a particle of size i, the particle is moved from L_i to D_i and is considered dissolved. If the mass dissolved is less than the mass of the particle, the mass dissolved is subtracted from the particle mass and a new radius is calculated based on the true density of the API. This particle remains in the L_i compartment until the remaining mass is dissolved. The new particle radius, λ_j, is determined by:

$$\lambda_j(t) = \sqrt[3]{\frac{3m_j(t)}{4\pi\rho_s}} \tag{9}$$

where $m_j(t)$ is the mass of the jth particle at time t, and ρ_s is the true density of the API.

The surface area available for dissolution within a given size class, $A_i(t)$, is then calculated as the surface area of all particles currently in the disintegrated compartment, L_i:

$$A_i(t) = \sum_j 4\pi \lambda_j(t)^2, \tag{10}$$

where $j = L_i(t)$ and $\lambda_j(t)$ is the radius of the jth particle at time, t.

The thickness of the unstirred media layer, $h_{t,i}$, can be calculated by:

$$h_{t,i} = \frac{2r_i}{Sh}, \tag{11}$$

where Sh is the Sherwood number. This was approximated for spherical particles by Ranz and Marshall (1952):

$$Sh = 2 + 0.6Re_p^{1/2} Sc^{1/3}, \tag{12}$$

where Re_p is the Reynolds number of the particle in the vessel, and $Sc = \nu/D_u$ is the Schmidt number, where ν is the kinematic viscosity of the media given by $\nu = \mu_T / \rho_{f,T}$. μ_T is the dynamic viscosity, and $\rho_{f,T}$ is the density of the media at temperature, T.

The Reynolds number, Re_p, is determined by:

$$Re_p = \frac{2r_i v_{r,t}}{\nu}, \tag{13}$$

where $v_{r,t}$ is the relative total velocity of the particle in the fluid:

$$v_{r,t} = \sqrt{v_t^2 + v_m^2}, \tag{14}$$

where v_t is the particle slip velocity and v_m is the relative velocities due to micro-eddies.

$$v_t = \frac{2r_i^2(\rho_s - \rho_{f,T})g}{18\mu_T}, \tag{15}$$

$$v_m = 0.195(2r_i)^{1.1} \epsilon^{0.525} \mu_T^{-0.575}, \tag{16}$$

where ρ_s is the true density of the API, g is gravitational acceleration at the surface of the Earth and ϵ is the power input for the USP II apparatus per unit of mass, defined as

$$\epsilon = P_0 \frac{\omega}{60}^3 \frac{D_p^5}{V_L}, \tag{17}$$

with ω as the paddle speed (in rpm), D_p as the paddle diameter, and P_0 as the power number of the USP II paddle. More details on the hydrodynamics within the USP II (paddle) apparatus are given by Sugano (2008).

The diffusion coefficient, D_u, is given by the Stokes–Einstein equation:

$$D_u = \frac{kT}{6\pi\mu_T r_h}, \tag{18}$$

where k is the Boltzmann constant, T is the absolute temperature, and r_h is the hydrated radius of the particle. The hydrated radius of the API particle, r_h is given by:

$$r_h = \sqrt[3]{\frac{3M_w}{4\pi N \rho_s}}, \tag{19}$$

where M_w is the molecular weight of the API and N is Avogadro's number.

2.3.4. Optimisation of model fitting parameters

The model optimisation was performed using the L-BFGS-B algorithm implemented in Python 3 using the SciPy package (Byrd et al., 1995; Zhu et al., 1997) to obtain values for the fitting parameters α, β_0, and $\beta_{t,0}$. The optimisation was performed to determine a single value for α for each API, and to obtain individual values for β_0 and $\beta_{t,0}$ for each batch. For each formulation, the optimisation was performed in parallel for all batches in order to increase the robustness of the parameter estimation.

To allow optimisation of the fitting parameters, the fitting parameter optimisation was bound between 1×10^{-8} and 1 for all parameters.

2.3.5. Assessment of model performance

To assess the performance of the model, the relative root mean square error (RRMSE) between the modelled and experimental dissolution profiles was calculated, according to:

$$RRMSE = \frac{\sqrt{\frac{1}{n} \sum_{t=1}^n (T_t - R_t)^2}}{\bar{R}_t} \tag{20}$$

where n is the number of sampling points.

In addition to the RRMSE, the dissolution model was also assessed by calculating the similarity factor (f2), the average fold error (AFE), and the absolute average fold error (AAFE). A summary of all error values is provided in Table S2 in the Supporting Information.
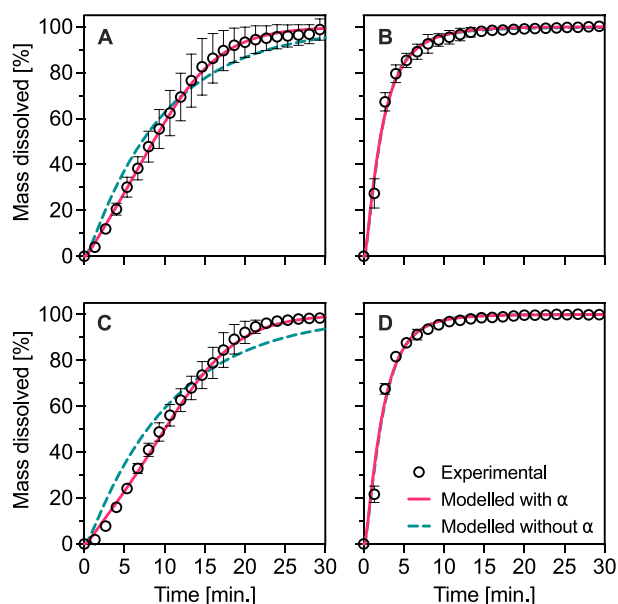
Fig. 2. The experimental and modelled dissolution profiles of tablets containing 1% wt. ibuprofen (top) and 10% wt. ibuprofen (bottom) at low porosity, B1, (A, C) and high porosity, B5 (B, D). The experimental profiles show the mean and standard deviation of $n = 6$ tablets, as reported by Bawuah et al. (2021). The modelled dissolution profiles with and without α in B and D directly overlap.

Fig. 3. The relative root mean square error (RRMSE) between the experimental and modelled dissolution profiles when the model is optimised both with and without the inclusion of the dissolution feedback parameter, α. The RRMSE is shown for tablets containing ibuprofen at (A) 1% and (B) 10% wt. drug loading, and tablets containing indomethacin at (C) 1% and (D) 10% wt. drug loading.

3. Results & discussion

3.1. Model performance

The experimental and modelled dissolution profiles are shown in Fig. 2 for tablets containing 1% and 10% wt. ibuprofen for batches B1 and B5, i.e. the lowest and highest porosity batches. The dissolution profiles of all ibuprofen and indomethacin batches are shown in Figures S2 and S3 of the Supporting Information. These profiles were generated by optimising the β_0 and $\beta_{t,0}$ parameters both with and without the inclusion of the α parameter, which describes the effect of the volume of dissolved drug on the disintegration rate. Using the multi-batch optimisation approach to obtain a single value of α for each API, α values of 0.00382 s^{-1} and 0.00016 s^{-1} were found for ibuprofen and indomethacin, respectively. From the dissolution profiles shown in Fig. 2A and C, it is clear that including the α parameter provides a profile shape which more accurately reflects the experimental profiles. For the highest porosity batches of ibuprofen, shown in Fig. 2B and D, the model gives similar profiles with and without the inclusion of the α term. This could suggest that the improvement in fit as a result of α is dependent on the mechanism of disintegration. In general, the dissolution model performs well, with the modelled profiles closely fitting the experimental profiles and remaining within the variability of the experimental data.

The performance of the model was evaluated by calculating the RRMSE between the experimental and modelled dissolution profiles. The RRMSE is shown in Fig. 3 for all batches of ibuprofen and indomethacin, both with and without the inclusion of the α parameter. For all batches, the RRMSE is below 3.5% when the α term is included, indicating good agreement between the experimental and modelled dissolution profiles. The dissolution model is able to capture the shape of the dissolution curve more accurately with the inclusion of the α parameter, which accounts for the effect of the volume of the drug which has already dissolved on the subsequent disintegration rate. During disintegration, the pore structure of the tablet is constantly evolving as a result of both the swelling of disintegrants and other
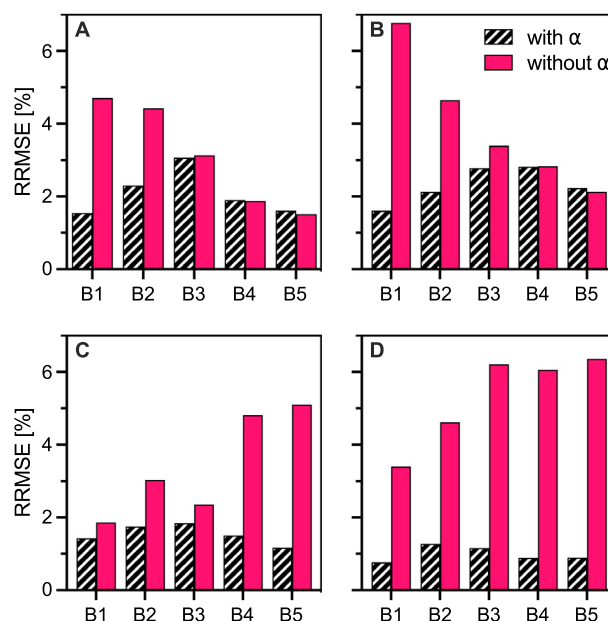
swelling excipients, and the dissolution of the API and soluble excipients. Comparing the effect of α on the model performance for each API, α offers the largest reduction in error for low porosity tablets containing indomethacin, whilst for ibuprofen α generally has a greater impact on the model performance at higher porosity levels. This could indicate that the effect of α is related to the API solubility and disintegration mechanism.

In addition to the RRMSE, the model performance was also assessed by calculating the f2 similarity factor, AFE and AAFE. The results of these additional error calculation are summarised in Table S2 of the Supporting Information. Overall, inclusion of the α parameter results in either an improved fit of the modelled profile to the experimental profile, or an identical profile to the curve generated without including the α term.

3.2. Movement between the compartments

The dissolution model provides the number of particles in each compartment at each time step, allowing for evaluation of the effect of particle size on the rate of movement of particles between compartments. Since it is assumed that the API is homogeneously distributed throughout the tablet, the relative number of particles released by disintegration at each time step is the same for every size bin. For example, normalising the number of particles in the Bound compartment over time would produce the same curve across each size bin.

Particles remain in the Disintegrated compartment from the time that they are released from the tablet by disintegration until the time that the particle has fully dissolved. For small particles, dissolution will be fast and the residence time of particles in the Disintegrated compartment will be very short. For these smaller size bins, particles will move almost immediately from the Bound to the Dissolved compartment, as demonstrated by the 0.1 μm particle size bin of indomethacin in Fig. 4A. On the other hand, larger particles will dissolve more slowly. In cases where particles are being released by disintegration faster than they are dissolving (i.e. large particles of a poorly-soluble drug), particles will begin to accumulate within the Disintegrated compartment. This is demonstrated for the larger size bins of indomethacin in Fig. 4B and C.
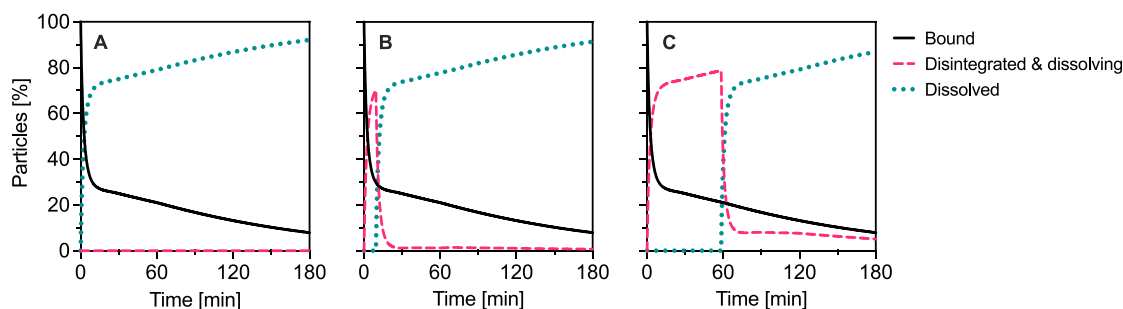
Fig. 4. The movement of API particles between compartments for tablets containing 10% wt. indomethacin with 21% porosity (B5 in Table 3). The movement of particles between compartments is shown for the (A) 0.1 μm, (B) 25.3 μm, and (C) 73.8 μm particle size bins. The number of particles is shown as the percentage of the total particles in each size class.

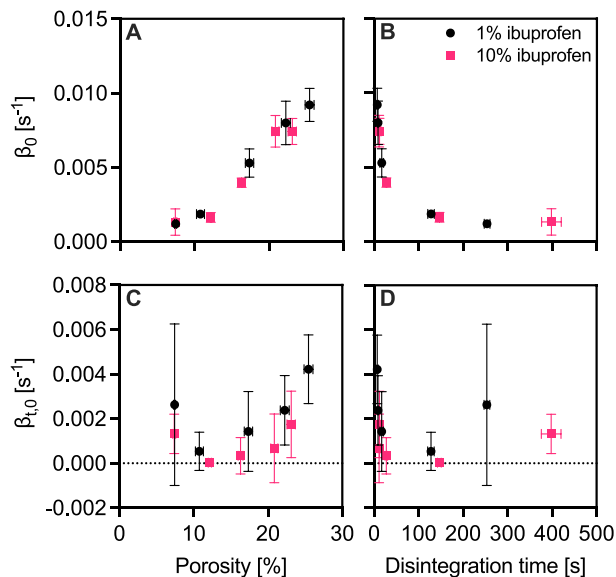**Fig. 5.** The correlation between the optimised fitting parameters, (top: A, B) β_0 and (bottom: C, D) $\beta_{t,0}$, with the (left: A, C) tablet porosity and (right: B, D) disintegration time for tablets containing 1% and 10% wt. ibuprofen. Values shown are the mean and standard deviation of $n = 6$ tablets (dissolution parameters and disintegration times), and $n = 10$ tablets (porosity).
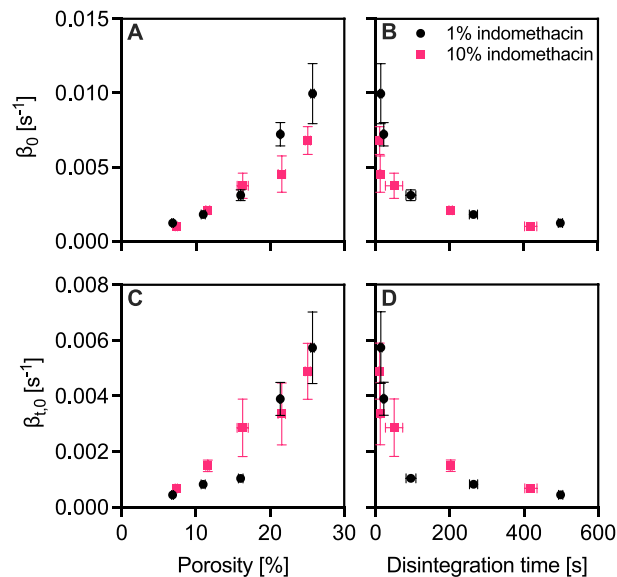
Fig. 6. The correlation between the optimised fitting parameters, (top: A, B) β_0 and (bottom: C, D) $\beta_{t,0}$, with the (left: A, C) tablet porosity and (right: B, D) disintegration time for tablets containing 1% and 10% wt. indomethacin. Values shown are the mean and standard deviation of $n = 6$ tablets (dissolution parameters and disintegration times), and $n = 10$ tablets (porosity).

3.3. Understanding the fitting parameters

The fitting parameters of ibuprofen and indomethacin tablets are shown in Figs. 5 and 6, respectively. During the optimisation, α was optimised to determine one value for each API. The disintegration parameters, β_0 and $\beta_{t,0}$, capture the differences in performance between different formulations or manufacturing conditions.

For the ibuprofen tablets, β_0 shows a strong correlation with porosity. As tablet porosity increases, there is a corresponding elevation in the initial disintegration rate, β_0, attributed to the enhanced rate at which liquid permeates the microstructural pores within the tablet. If the correlation between porosity and β_0 is considered to be linear, R^2 values of 98.8% and 92.1% are obtained for tablets of 1% and 10% wt. ibuprofen, respectively.

The decay rate parameter, $\beta_{t,0}$, increases with porosity in a non-linear fashion at porosity levels above approximately 5%. In the case of the lowest porosity batch, it is possible that the disintegration mechanism changes compared to the other batches, for example, the disintegration is more similar to an eroding tablet. The $\beta_{t,0}$ parameter also shows much higher variability compared to β_t and the fitting parameters for indomethacin. As discussed later in this section, $\beta_{t,0}$ does not appear to have a particularly strong effect on the dissolution of these ibuprofen tablets, i.e. the model is not sensitive to this parameter in the case of ibuprofen.

The indomethacin tablets also demonstrate positive correlations between both β_0 and $\beta_{t,0}$ with porosity. At 10% wt. drug loading, the correlation is linear within the porosity range studied, with an R^2 of 97.0% and 96.2% for β_0 and $\beta_{t,0}$, respectively. In the case of tablets containing 1% wt. indomethacin, the relationship between β_0 and $\beta_{t,0}$ concerning porosity does not follow a strictly linear trend. This could be attributed to a shift in the dominant mechanisms governing performance-related disintegration behaviours within the range of 12% to 16% porosity.

To investigate the sensitivity of the dissolution profile to the fitting parameters, β_0 and $\beta_{t,0}$, dissolution profiles were generated for 100 different values of β_0 ranging from 1×10^{-11} to 0.010, each combined with 100 values of $\beta_{t,0}$ values ranging from 0 to 0.006. The time to reach 50 and 80% dissolution (t_{50} and t_{80}) for each 10% wt. simulated profile is shown in Figs. 7 and 8 for indomethacin and ibuprofen, respectively.

Due to the low solubility of indomethacin, low values of β_0 and high values of $\beta_{t,0}$ (which describe slow disintegration, i.e. the slow release of particles from the Bound compartment to the Disintegrated and Dissolving compartment), results in slow dissolution. In the case of indomethacin, profiles were simulated up to the 480 min timepoint. In
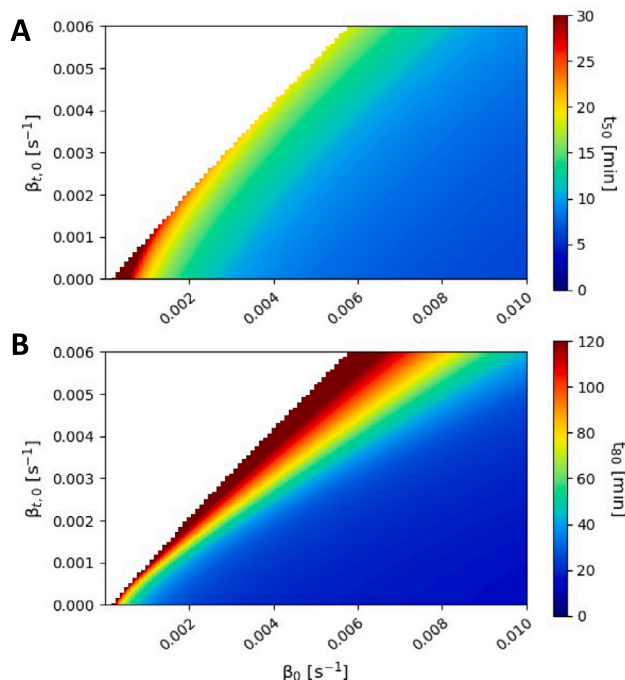
Fig. 7. The time to reach (A) 50% dissolution (t_{50}), and (B) 80% dissolution (t_{80}) for batches of 10% wt. indomethacin with different values for the disintegration rate parameters, β_0 and $\beta_{t,0}$. Combinations which result in an incomplete dissolution profile (i.e. <100% dissolution) after 480 min are excluded.
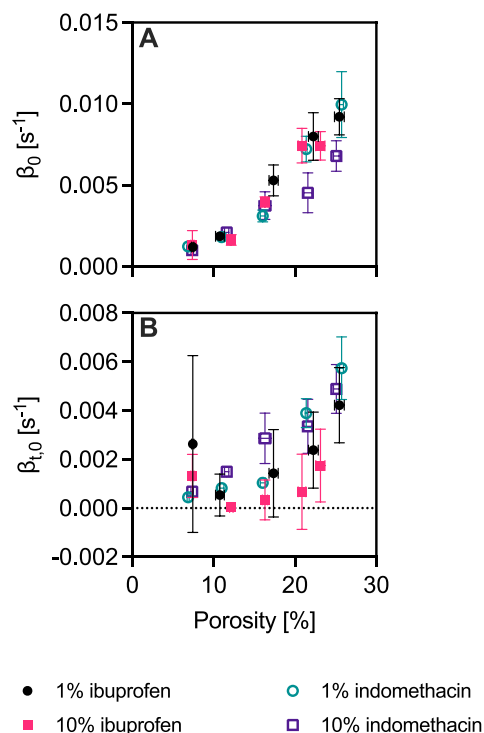

Fig. 9. The (A) β_0 and (B) $\beta_{t,0}$ fitting parameters for all batches of ibuprofen and indomethacin tablets.
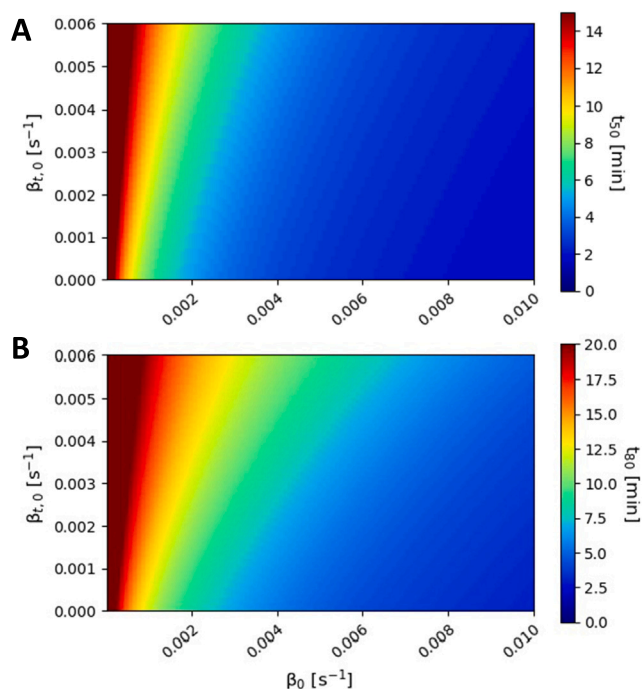

Fig. 8. The time to reach (A) 50% dissolution (t_{50}), and (B) 80% dissolution (t_{80}) for batches of 10% wt. ibuprofen with different values for the disintegration rate parameters, β_0 and $\beta_{t,0}$.

Based on Figs. 7 and 8, the two different API demonstrate different dissolution behaviour. For indomethacin, both β_0 and $\beta_{t,0}$ will influence the dissolution performance. On the other hand, the t_{50} and t_{80} values obtained from ibuprofen profiles demonstrate a much lower dependence on $\beta_{t,0}$ compared to β_0, suggesting that disintegration and dissolution are primarily driven by the initial rate of liquid penetration. In both cases, the heatmaps reveal zones within which changing the fitting parameters has little effect on the t_{50} and t_{80}. In these regions, the performance of the tablet is no longer limited by the disintegration of the tablet, but is now limited by the dissolution rate.

3.4. Potential applications

The proposed dissolution model could have a diverse range of applications within drug product development, from early stage formulation and development activities, through to real-time release testing of batches for the market.

3.4.1. Early development tool

During the early stages of development, there may be limited amounts of API available. For this reason, experiments must be selected strategically in order to maximise the product understanding with the material available. The input parameters of this dissolution model are raw material properties which are routinely collected during development (e.g. the true density, solubility and PSD of the API). The model could be used as a pre-screening tool to identify the formulations and manufacturing conditions which are most likely to produce the desired dissolution performance, as determined in the Quality Target Product Profile (QTPP) (Yu et al., 2014). Where dissolution data is not yet available to determine the fitting parameters, values of β_0 and $\beta_{t,0}$ could be estimated based on previous knowledge of similar formulations, in order to predict the dissolution performance of a product with a

cases where the dissolution profile was incomplete and did not reach 100% within 480 min, the t_{50} and t_{80} are not included.

new API in the same formulation. These predictions could be used to select formulations most likely to be successful as a starting point for experimental screening.

The disintegration rate parameters of all MCC/lactose-based tablets are shown in Fig. 9. The initial disintegration rate parameter, β_0, is similar for MCC/lactose-based tablets containing 1 and 10% wt. ibuprofen and indomethacin, despite the different API and drug loadings of these formulations. This is not the case for the decay rate parameter, $\beta_{t,0}$, due to the fact that the dissolution performance of ibuprofen is not sensitive to changes in $\beta_{t,0}$. These results suggest that the fitting parameters of MCC/lactose-based indomethacin tablets could potentially be used to provide an initial estimation of the dissolution performance of tablets with the same formulation and a new API. To make these predictions, the dissolution feedback parameter, α, must be known, and so further work is required to establish whether α could be determined based on the raw material properties of the API.

3.4.2. Assessment of process changes

Aside from being a tool to screen formulations, this model could be used to evaluate the risk associated with changes in the raw material properties or processing conditions of the API. For example, the model could be used to assess the impact of changes in the PSD of the API as a result of changes to the crystallisation process or the addition of a milling stage. Whilst these predictions would require validation with experimental data, they could provide an estimation of which process changes maintain an acceptable dissolution performance, in order to reduce the amount of experimental work required, thereby also reducing the associated time and materials required.

3.4.3. Implementing real-time release testing

This dissolution model also shows potential for enabling real-time release testing (RTRT) in a continuous direct compression (CDC) manufacturing line. NIR and Raman spectroscopy have already been demonstrated as tools to measure the drug loading in continuous manufacturing lines (Goodwin et al., 2018; Shimamura et al., 2019; Belay et al., 2021). In addition to enabling the assessment of content uniformity, these measurements could directly feed into the model to provide the exact drug loading. By exploiting the correlations observed between porosity and the fitting parameters of these batches, dissolution profiles could be predicted based on at-line or in-line measurements of porosity within the CDC line, for example, using non-destructive techniques such as terahertz time-domain spectroscopy (THz-TDS) to monitor tablet thickness and porosity (Bawuah et al., 2023; Anuschek et al., 2023). In contrast to most RTRT approaches, which rely on multivariate analysis or machine learning, this method relies primarily on raw material properties of the API, with only a small number of experimental data points required to calibrate the model fitting parameters against the relevant parameter, e.g. porosity.

4. Conclusions

The compartmental model presented in this study uses population-balance principles to model the disintegration and dissolution process for directly compressed tablets. The data used in this study for ibuprofen and indomethacin tablets demonstrates the ability to isolate the effects of the manufacturing conditions (i.e. compression force) in the disintegration fitting parameters, β_0 and $\beta_{t,0}$. As this model primarily uses raw material properties as inputs (PSD, true density, and solubility of the API), it can be applied without the need for large experimental datasets. Additionally, the use of a multi-batch optimisation approach enables robust parameter estimation across a range of porosity levels for a given formulation.

This model shows potential for use in both drug product development or as part of a real-time release testing (RTRT) control strategy, however, future work is required to examine larger datasets to explore whether the model is able to accurately capture the effect of changes

in the PSD, and whether the fitting parameters would be transferrable to new products using the same formulation with a new API. Further, the α parameter is treated as an API property in this study, and further data is required to assess whether a single α value is still applicable to an API after micronisation, or at a much higher drug loading.

CRediT authorship contribution statement

Natalie Maclean: Writing – original draft, Software, Methodology, Investigation, Formal analysis, Data curation, Conceptualization. **John A. Armstrong:** Writing – review & editing, Software, Methodology, Conceptualization. **Mark A. Carroll:** Writing – review & editing, Software, Methodology, Conceptualization. **Mohammad Salehian:** Writing – review & editing, Software, Methodology, Conceptualization. **James Mann:** Writing – review & editing, Supervision, Conceptualization. **Gavin Reynolds:** Writing – review & editing, Supervision, Conceptualization. **Blair Johnston:** Writing – review & editing, Supervision, Funding acquisition. **Daniel Markl:** Writing – review & editing, Supervision, Methodology, Funding acquisition, Conceptualization.

Declaration of competing interest

The authors declare that they have no known competing financial interests or personal relationships that could have appeared to influence the work reported in this paper.

Data availability

The dataset for this paper is available online via the University of Strathclyde repository at https://doi.org/10.15129/0de30626-a898-42a5-9548-342a748062bc.

Appendix A. Supplementary data

Supplementary material related to this article can be found online at https://doi.org/10.1016/j.ijpharm.2024.124084.

References

Anuschek, M., Kvistgaard Vilhelmsen, T., Axel Zeitler, J., Rantanen, J., 2023. Towards simultaneous determination of tablet porosity and height by terahertz time-domain reflection spectroscopy. Int. J. Pharm. (ISSN: 0378-5173) 123424. http://dx.doi.org/10.1016/j.ijpharm.2023.123424.

Bawuah, P., Evans, M., Lura, A., Farrell, D.J., Barrie, P.J., Kleinebudde, P., Markl, D., Zeitler, J.A., 2023. At-line porosity sensing for non-destructive disintegration testing in immediate release tablets. Int. J. Pharm.: X (ISSN: 2590-1567) 5, 100186. http://dx.doi.org/10.1016/j.ijpx.2023.100186.

Bawuah, P., Markl, D., Turner, A., Evans, M., Portieri, A., Farrell, D., Lucas, R., Anderson, A., Goodwin, D.J., Zeitler, J.A., 2021. A fast and non-destructive terahertz dissolution assay for immediate release tablets. J. Pharm. Sci. (ISSN: 0022-3549) 110 (5), 2083–2092. http://dx.doi.org/10.1016/j.xphs.2020.11.041.

Belay, N.F., Busche, S., Manici, V., Shaukat, M., Arndt, S., Schmidt, C., 2021. Evaluation of transmission raman spectroscopy and nir hyperspectral imaging for the assessment of content uniformity in solid oral dosage forms. Eur. J. Pharm. Sci. (ISSN: 0928-0987) 166, 105963. http://dx.doi.org/10.1016/j.ejps.2021.105963.

Berardi, A., Bisharat, L., Quodbach, J., Abdel Rahim, S., Perinelli, D.R., Cespi, M., 2021. Advancing the understanding of the tablet disintegration phenomenon – an update on recent studies. Int. J. Pharm. (ISSN: 0378-5173) 598, 120390. http://dx.doi.org/10.1016/j.ijpharm.2021.120390.

Brunner, E., 1904. Reaktionsgeschwindigkeit in heterogenen systemen. Z. Phys. Chem. 47U (1), 56–102. http://dx.doi.org/10.1515/zpch-1904-4705.

Byrd, R.H., Lu, P., Nocedal, J., Zhu, C., 1995. A limited memory algorithm for bound constrained optimization. SIAM J. Sci. Comput. 16 (5), 1190–1208. http://dx.doi.org/10.1137/0916069, ISSN 1064-8275, 1095-7197.

Desai, P.M., Liew, C.V., Heng, P.W.S., 2016. Review of disintegrants and the disintegration phenomena. J. Pharm. Sci. (ISSN: 0022-3549) 105 (9), 2545–2555. http://dx.doi.org/10.1016/j.xphs.2015.12.019.

Djukaj, S., Kolář, J., Lehocký, R., Zadražil, A., Štěpánek, F., 2022. Design of particle size distribution for custom dissolution profiles by solving the inverse problem. Powder Technol. (ISSN: 0032-5910) 395, 743–757. http://dx.doi.org/10.1016/j.powtec.2021.10.023.

Dumarey, M., Goodwin, D.J., Davison, C., 2015. Multivariate modelling to study the effect of the manufacturing process on the complete tablet dissolution profile. Int. J. Pharm. (ISSN: 0378-5173) 486 (1), 112–120. http://dx.doi.org/10.1016/j.ijpharm.2015.03.040.

FDA, 1997. Guidance for industry: Dissolution testing of immediate release solid oral dosage forms.

Ferdoush, S., Gonzalez, M., 2023. Semi-mechanistic reduced order model of pharmaceutical tablet dissolution for enabling industry 4.0 manufacturing systems. Int. J. Pharm. (ISSN: 0378-5173) 631, 122502. http://dx.doi.org/10.1016/j.ijpharm.2022.122502.

Fink, E., Celikovic, S., Rehrl, J., Sacher, S., Afonso Urich, J.A., Khinast, J., 2023. Prediction of dissolution performance of uncoated solid oral dosage forms via optical coherence tomography. Eur. J. Pharmaceut. Biopharmaceut. (ISSN: 0939-6411) 189, 281–290. http://dx.doi.org/10.1016/j.ejpb.2023.07.003.

Freitas, M.P., Sabadin, A., Silva, L.M., Giannotti, F.M., do Couto, D.A., Tonhi, E., Medeiros, R.S., Coco, G.L., Russo, V.F.T., Martins, J.A., 2005. Prediction of drug dissolution profiles from tablets using nir diffuse reflectance spectroscopy: A rapid and nondestructive method. J. Pharm. Biomed. Anal. (ISSN: 0731-7085) 39 (1), 17–21. http://dx.doi.org/10.1016/j.jpba.2005.03.023.

Galata, D.L., Farkas, A., Könyves, Z., Mészáros, L.A., Szabó, Edina, Csontos, I., Pálos, A., Marosi, G., Nagy, Z.K., Nagy, B., 2019. Fast, spectroscopy-based prediction of in vitro dissolution profile of extended release tablets using artificial neural networks. Pharmaceutics (ISSN: 1999-4923) 11 (88), 400. http://dx.doi.org/10.3390/pharmaceutics11080400.

Galata, D.L., Könyves, Z., Nagy, B., Novák, M., Mészáros, L.A., Szabó, E., Farkas, A., Marosi, G., Nagy, Z.K., 2021. Real-time release testing of dissolution based on surrogate models developed by machine learning algorithms using nir spectra, compression force and particle size distribution as input data. Int. J. Pharm. (ISSN: 0378-5173) 597 (120338), http://dx.doi.org/10.1016/j.ijpharm.2021.120338.

Galata, D.L., Zsiros, B., Knyihár, G., Péterfi, O., Mészáros, L.A., Ronkay, F., Nagy, B., Szabó, E., Nagy, Z.K., Farkas, A., 2023. Convolutional neural network-based evaluation of chemical maps obtained by fast raman imaging for prediction of tablet dissolution profiles. Int. J. Pharm. (ISSN: 0378-5173) 640, 123001. http://dx.doi.org/10.1016/j.ijpharm.2023.123001.

Galata, D.L., Zsiros, B., Mészáros, L.A., Nagy, B., Szabó, E., Farkas, A., Nagy, Z.K., 2022. Raman mapping-based non-destructive dissolution prediction of sustained-release tablets. J. Pharm. Biomed. Anal. (ISSN: 0731-7085) 212, 114661. http://dx.doi.org/10.1016/j.jpba.2022.114661.

Goodwin, D.J., van den Ban, S., Denham, M., Barylski, I., 2018. Real time release testing of tablet content and content uniformity. Int. J. Pharm. (ISSN: 0378-5173) 537 (1), 183–192. http://dx.doi.org/10.1016/j.ijpharm.2017.12.011.

Hernandez, E., Pawar, P., Keyvan, G., Wang, Y., Velez, N., Callegari, G., Cuitino, A., Michniak-Kohn, B., Muzzio, F.J., Romañach, R.J., 2016. Prediction of dissolution profiles by non-destructive near infrared spectroscopy in tablets subjected to different levels of strain. J. Pharm. Biomed. Anal. (ISSN: 0731-7085) 117, 568–576. http://dx.doi.org/10.1016/j.jpba.2015.10.012.

ICH, 2009. Q8(R2) pharmaceutical development.

Jange, C.G., Wassgren, C.R., Ambrose, K., 2023. The significance of tablet internal structure on disintegration and dissolution of immediate-release formulas: A review. Powders (ISSN: 2674-0516) 2 (11), 99–123. http://dx.doi.org/10.3390/powders2010008.

Kapoor, Y., Meyer, R.F., Ferguson, H.M., Skomski, D., Daublain, P., Troup, G.M., Dalton, C., Ramasamy, M., Templeton, A.C., 2021. Flexibility in drug product development: A perspective. Mol. Pharm. 18 (7), 2455–2469. http://dx.doi.org/10.1021/acs.molpharmaceut.1c00210, ISSN 1543-8384, 1543-8392.

Maclean, N., Walsh, E., Soundaranathan, M., Khadra, I., Mann, J., Williams, H., Markl, D., 2021. Exploring the performance-controlling tablet disintegration mechanisms for direct compression formulations. Int. J. Pharm. (ISSN: 0378-5173) 599, 120221. http://dx.doi.org/10.1016/j.ijpharm.2021.120221.

Markl, D., Warman, M., Dumarey, M., Bergman, E., Folestad, S., Shi, Z., Manley, L.F., Goodwin, D.J., Zeitler, J.A., 2020. Review of real-time release testing of pharmaceutical tablets: State-of-the art, challenges and future perspective. Int. J. Pharm. (ISSN: 0378-5173) 582, 119353. http://dx.doi.org/10.1016/j.ijpharm.2020.119353.

Markl, D., Zeitler, J.A., 2017. A review of disintegration mechanisms and measurement techniques. Pharm. Res. (ISSN: 1573-904X) 34 (5), 890–917. http://dx.doi.org/10.1007/s11095-017-2129-z.

Matsunami, K., Miura, T., Yaginuma, K., Tanabe, S., Badr, S., Sugiyama, H., 2023. Surrogate modeling of dissolution behavior toward efficient design of tablet manufacturing processes. Comput. Chem. Eng. (ISSN: 0098-1354) 171, 108141. http://dx.doi.org/10.1016/j.compchemeng.2023.108141.

Nagy, B., Szabados-Nacsa, Á., Fülöp, G., Turák Nagyné, A., Galata, D.L., Farkas, A., Mészáros, L.A., Nagy, Z.K., Marosi, G., 2023. Interpretable artificial neural networks for retrospective qbd of pharmaceutical tablet manufacturing based on a pilot-scale developmental dataset. Int. J. Pharm. (ISSN: 0378-5173) 633, 122620. http://dx.doi.org/10.1016/j.ijpharm.2023.122620.

Péterfi, O., Nagy, Z.K., Sipos, E., Galata, D.L., 2023. Artificial intelligence-based prediction of in vitro dissolution profile of immediate release tablets with near-infrared and raman spectroscopy. Period. Polytech. Chem. Eng. (ISSN: 1587-3765) 67 (11), 18–30. http://dx.doi.org/10.3311/PPch.20755.

Quodbach, J., Kleinebudde, P., 2015. A critical review on tablet disintegration. Pharm. Dev. Technol. 1–12. http://dx.doi.org/10.3109/10837450.2015.1045618, ISSN 1083-7450, 1097-9867.

Ranz, W.E., Marshall, W.R., 1952. Evaporation from drops. Chem. Eng. Prog. 48 (141–146), 173–180.

Shimamura, R., Koide, T., Hisada, H., Inoue, M., Fukami, T., Katori, N., Goda, Y., 2019. Pharmaceutical quantification with univariate analysis using transmission raman spectroscopy. Drug Dev. Ind. Pharm. (ISSN: 0363-9045) 45 (9), 1430–1436. http://dx.doi.org/10.1080/03639045.2019.1621336.

Sugano, K., 2008. Theoretical comparison of hydrodynamic diffusion layer models used for dissolution simulation in drug discovery and development. Int. J. Pharm. (ISSN: 0378-5173) 363 (1), 73–77. http://dx.doi.org/10.1016/j.ijpharm.2008.07.002.

Weiss, H., 2013. The sir model and the foundations of public health. Mater. Mat. (ISSN: 1887-1097) 0001–0017.

Wilson, D., Wren, S., Reynolds, G., 2012. Linking dissolution to disintegration in immediate release tablets using image analysis and a population balance modelling approach. Pharm. Res. 29 (1), 198–208. http://dx.doi.org/10.1007/s11095-011-0535-1, ISSN 0724-8741, 1573-904X.

Yu, L.X., Amidon, G., Khan, M.A., Hoag, S.W., Polli, J., Raju, G.K., Woodcock, J., 2014. Understanding pharmaceutical quality by design. AAPS J. (ISSN: 1550-7416) 16 (4), 771–783. http://dx.doi.org/10.1208/s12248-014-9598-3.

Zaborenko, N., Shi, Z., Corredor, C.C., Smith-Goettler, B.M., Zhang, L., Hermans, A., Neu, C.M., Alam, M.A., Cohen, M.J., Lu, X., Xiong, L., Zacour, B.M., 2019. First-principles and empirical approaches to predicting in vitro dissolution for pharmaceutical formulation and process development and for product release testing. AAPS J. (ISSN: 1550-7416) 21 (3), 32. http://dx.doi.org/10.1208/s12248-019-0297-y.

Zhu, C., Byrd, R.H., Lu, P., Nocedal, J., 1997. Algorithm 778: L-bfgs-b: Fortran subroutines for large-scale bound-constrained optimization. ACM Trans. Math. Software 23 (4), 550–560. http://dx.doi.org/10.1145/279232.279236, ISSN 0098-3500, 1557-7295.